Model-based upper-limb gravity compensation strategies for active dynamic arm supports

Maxime Manzano, Sylvain Guégan, Ronan Le Breton, Louise Devigne, Marie Babel

Model-based upper-limb gravity compensation strategies for active dynamic arm supports

Maxime Manzano[1], Sylvain Guégan[2], Ronan Le Breton[2], Louise Devigne[3] and Marie Babel[1]

***Abstract*— Neuromuscular disorders (NMDs) may induce difficulties to perform daily life activities in autonomy. For people with NMDs affecting the upper-limb mobility, dynamic arm supports (DASs) turn out to be relevant assistive devices. In particular, active DASs benefit from an external power source to support severely impaired people. However, commercially available active devices are controlled with push buttons, which adds cognitive load and discomfort. To alleviate this issue, we propose a new force-based assistive control framework. In this preliminary work, we focus on the computation of a feedforward force to compensate upper-limb gravity. Four strategies based on a biomechanical model of the upper limb, tuned using anthropometric measurements, are proposed and evaluated. The first one is based on the potential energy of the upper-limb, the second one makes a compromise between the shoulder and elbow torques, the third one minimizes the sum of the squared user joint torques and the last one uses a probabilistic approach to minimize the expected torque norm in the presence of model uncertainties. These strategies have been evaluated quantitatively through an experiment including nine participants with an active DAS prototype. The activity of six muscles was measured and used to compute the mean effort index (MEI) which represents the global effort required to maintain the pose. A statistical analysis shows that the four strategies significantly lower the MEI (p-value < 0.001).**

Keywords: Dynamic arm support, Assistive robotics, Assistive control, Force control, Neuromuscular disorders, Upper-limb gravity compensation.

I. INTRODUCTION

Neuromuscular disorders (NMDs) include troubles in the nerves, the muscles or the communication between both. These troubles may come from different diseases such as multiple sclerosis or spinal cord injury. When the upper-limb is affected, the autonomy is reduced and performing independently Activities of Daily Living (ADLs) such as washing or eating, and more generally reaching and grasping objects, can be challenging. In such situations, Assistive Devices (ADs) provide a solution to keep performing ADLs with autonomy.

Many ADs are already available to compensate for mobility impairments induced by upper-limb weakness. On the one hand, there exists task-specific devices such as meal assistance robots [1]. Some of them are designed to support users with tremor while others are designed for people with upper-limb muscle weaknesses. On the other hand, robotic manipulators such as the Jaco robotic arm from Kinova enable people with low mobility to keep their autonomy in a larger set of ADLs as it allows not only to eat by oneself but also to remotely manipulate objects [2]. However, the price of such a device limits its number of users. Moreover, keeping using the upper-limb may delay the loss of mobility for people with muscular dystrophy [3], which robotic arms do not permit. Between robotic arms and meal assistance robots, a promising family of ADs are dynamic arm supports (DAS), also called mobile arm supports. This technology supports the upper-limb of people, enabling them to perform many ADLs while keeping mobilizing their muscles. According to [4], the DASs can be classified in three main categories: non-actuated, passively actuated (or passive) and actively actuated (or active) devices. Non-actuated devices are made of passive joints that only block some motions to support the user's upper-limb. They are mainly used to relieve the arm while performing table-top activities. Passive DASs are able to store and give back mechanical energy thanks to components such as a spring or a counterweight. Lastly, active DASs have an external power input and generally support the forearm with a vertical force. A recent clinical study shows that passive DASs are effective for moderately impaired people, while severely impaired people only benefit from active DASs [5]. Moreover, if exoskeletons may be included in the active DASs [6], most of them are bulky because of many actuated joints and some of them require to be carried by the user which is hardly possible for people with NMDs. According to [5], the control system of active

Fig. 1: The active DAS prototype used to implement the four proposed strategies to compensate for the upper-limb weight.

[1]Univ Rennes, INSA Rennes, Inria, CNRS, IRISA - UMR 6074, F-35000 Rennes, France, maxime.manzano@insa-rennes.fr, marie.babel@irisa.fr

[2]Univ Rennes, INSA Rennes, LGCGM, F-35000 Rennes, France

[3]Univ Rennes, Inria, CNRS, IRISA - UMR 6074, F-35000 Rennes, France

DASs are not natural enough, which limits their effectiveness and acceptability among users. Indeed, they use push buttons to detect the user intent, which induces a high cognitive load and prevents users from using both of their upper-limbs. Moreover, the active DASs do not assist downward motions as they only support the upper-limb against gravity, which makes some activities even harder to perform such as pushing on a door handle. In a more general way, even though some studies already proved that DASs increase the abilities of people with NMDs, their efficiency in an everyday context is still discussed [7].

In this context, innovative control strategies are needed to ease the use of active DASs. These strategies may rely on sensors measuring physiological signals or on the user's residual motor abilities to efficiently detect user intent. [8] references a large panel of intention detection strategies dedicated to robotic upper-limb orthoses. For instance, an elbow orthosis was developed by [9] to implement a position-based control method: user intent is detected either from EMG signals or from voluntarily developed force measured on the DAS.

This paper proposes an innovative force-based control framework for active DASs that provide a vertical force to the forearm. In Section II, we present the general framework, a model of the user's upper-limb as well as four gravity compensation strategies based on this model. Then, the Section III presents the experiment that we performed with nine participants without NMDs to evaluate the four proposed strategies. The results are discussed in Section IV and we draw first conclusions as well as guidelines for future works in Section V.

II. MODEL-BASED CONTROL STRATEGIES

A. General force-based control framework

This paper proposes a force-based control framework for active DASs that provides a vertical force to the user's forearm. In this framework, the control is based on the force F^* which is the desired force to apply to the forearm. F^* is computed from two contribution as

$$F^* = F_g^* + F_i^*, \tag{1}$$

where F_i^* is the *intent* force and F_g^* is the *gravity* compensation force. F_i^* comes directly from the interpretation of user *intent* which is measured by sensors. This intent may be to move upward or downward, or to develop a force. F_g^* is a feedforward term that compensates for the gravity acting on the user's upper-limb.

This framework is designed to reduce the cognitive load of the user by removing the need for a manual controller to operate the DAS. Furthermore, if the user intent is properly detected, the active DAS is able to help him/her to develop a force, even if this force is downward. In this case, the total assistive force F^* will be reduced to benefit from the user's arm weight. This feature is not implemented in current DASs.

As a first step to implement the proposed force-based control framework, this paper only focuses on the F_g^* component. We propose four strategies to compute the gravity compensation force F_g^* based on a biomechanical model of the upper-limb.

B. Upper-limb and DAS mechanical model

The upper-limb is modeled as a planar serial robot with two rigid bodies (the upper-arm and the forearm), articulated at the shoulder and elbow (Fig. 2). The lengths and masses are noted l_{ua} and m_{ua} for the upper-arm and l_{fa} and m_{fa} for the forearm. We assume the Center of Mass (CoM) of these two bodies lies on their main axis. The distance from shoulder to the upper-arm CoM is $x_{G_{ua}}$ and the one from the elbow to the forearm CoM is $x_{G_{fa}}$. The shoulder and elbow flexion angles are q_s and q_e and the user's joint torques are τ_s and τ_e. The armrest is considered as the end-effector of this model (point P of Cartesian coordinates (x, y)). It is located on the forearm with respect to the elbow with parameters l_P longitudinally and h_P perpendicularly. The assistive force F is applied vertically to the user's forearm at this point P. This force is computed from the motor torque τ_m, the motor angle α_m and the DAS lever length l_m as

$$F = \frac{\tau_m}{l_m \cos \alpha_m}. \tag{2}$$

The motor position along the $\mathbf{x_0}$ axis is noted x_m.

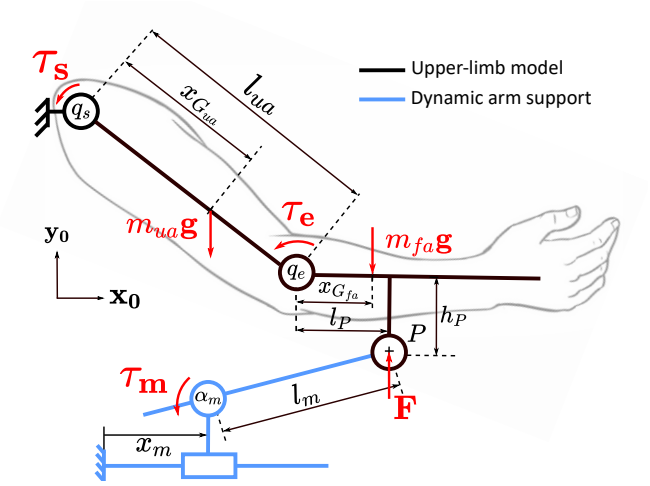

Fig. 2: Upper-limb and DAS static model. Bold text indicates vector quantities.

This model makes several simplifications. It considers rigid bodies and perfect joints with only one degree of freedom (DoF). It neglects the muscles and tendons which may induce friction. The shoulder is modeled as a ball-socket joint, neglecting some motions we are able to perform with our shoulder complex and trunk movements. Lastly, only planar motions are considered.

The Body Segment Inertial Parameters (BSIPs) of the upper-limb and forearm (i.e., $x_{G_{ua}}$, $x_{G_{fa}}$, m_{ua} and m_{fa}) are required to compute elbow and shoulder torques that are

at the origin of the gravity compensation strategies. Furthermore, the uncertainty of those parameters may be needed for some robust strategies. Six references from the literature were used to estimate those parameters [10]–[15]. They all use regression models to estimate the CoM positions and human body segment masses. The simplest ones compute the segment masses as a fraction of the human body mass and the CoMs as a fraction of the segment lengths [10]–[13]. The most recent works estimate those parameters with more anthropometric data such as the Body Mass Index (BMI), age and sex of the user [14], [15].

In this paper, the BSIPs are computed as the mean of the estimates given by [10]–[15]. The uncertainties are considered as the difference between the maximum and minimum values of these estimates. The anthropometric measurements required to estimate the BSIPs of the subjects are the sex, age, weight, BMI, the lengths of the upper-arm, forearm and hand as well as the circumferences of the upper-arm, forearm, elbow, waist and hip.

C. Strategies to compute the assistive force

F_g^* is computed to reduce both shoulder and elbow torques. τ_s and τ_e are estimated thanks to the proposed simplified model (Fig. 2) by applying the Newton's second law first to the forearm and then to the upper-arm. This gives the elbow and shoulder torque equations

$$\begin{cases} \tau_e = -F(l_P \cos(q_s+q_e) - h_P \sin(q_s+q_e)) \\ \qquad + m_{fa}\, g\, x_{G_{fa}} \cos(q_s+q_e), \\ \tau_s = \tau_e + (m_{ua}\, x_{G_{ua}} + m_{fa}\, l_{ua}) g \cos(q_s) \\ \qquad - F\, l_{ua} \cos(q_s). \end{cases} \tag{3}$$

with g the gravitational acceleration and F the support force.

To support both the shoulder and elbow torques, a first idea could be to zero τ_s since it is the highest one for many poses. However this strategy is not acceptable since there is a singularity when the point P is aligned vertically with the shoulder. Thus, we propose four strategies to compute the feedforward gravity compensation force F_g^* based on the mechanical model presented before. They all use the current pose (q_s, q_e) and the user's BSIPs as inputs.

1) Potential Energy Based (PEB) strategy: This first strategy is based on the design technique of some passive and hybrid DASs [16] which are design to have a constant potential energy. For this strategy, we compute the gravity compensation force as a conservative force, derived from a potential energy called U_{DAS}:

$$\mathbf{F_{PEB}} = -\mathbf{grad}(U_{DAS}), \tag{4}$$

with $\mathbf{F_{PEB}}$ the 2D gravity compensation force. Bold texts indicate vector quantities in the sagittal plane (Fig. 2). Alongside, we compute the upper-limb potential energy U_{UL} due to gravity as follow:

$$\begin{aligned} U_{UL} = {} & m_{fa} g \left(l_{ua} \sin(q_s) + x_{G_{fa}} \sin(q_s+q_e) \right) \\ & + m_{ua} g x_{G_{ua}} \sin(q_s). \end{aligned} \tag{5}$$

Then, we assume the total potential energy is equal to a constant U_0 such that

$$U_{UL} + U_{DAS} = U_0. \tag{6}$$

Since U_0 is constant, by differentiating Eq. (6) we get

$$-\mathbf{grad}(U_{DAS}) = \mathbf{grad}(U_{UL}) \Leftrightarrow \mathbf{F_{PEB}} = \begin{pmatrix} \frac{\partial U_{DAS}}{\partial x} \\ \frac{\partial U_{DAS}}{\partial y} \end{pmatrix} \tag{7}$$

The Jacobian of the upper-limb is used to differentiate U_{DAS}:

$$\mathbf{F_{PEB}} = J^{-T} \begin{pmatrix} \frac{\partial U_{DAS}}{\partial q_s} \\ \frac{\partial U_{DAS}}{\partial q_e} \end{pmatrix} \text{ with } J = \begin{pmatrix} \frac{\partial x}{\partial q_s} & \frac{\partial x}{\partial q_e} \\ \frac{\partial y}{\partial q_s} & \frac{\partial y}{\partial q_e} \end{pmatrix}. \tag{8}$$

The DASs studied in this paper can only generate a vertical force so this strategy is implemented by keeping only the term along $\mathbf{y_0}$ to compute F_g^*

$$F_g^* = \mathbf{F_{PEB}} \cdot \mathbf{y_0}. \tag{9}$$

The Jacobian matrix is computed by differentiating the Direct Geometric Model (DGM) of the upper-limb

$$\begin{cases} x = l_{ua} \cos q_s + l_P \cos q_{se} - h_P \sin q_{se}, \\ y = l_{ua} \sin q_s + l_P \sin q_{se} + h_P \cos q_{se}, \end{cases} \tag{10}$$

with $q_{se} = q_s + q_e$.

2) Motor Ability Based (MAB) strategy: According to Eq. (3), the operating point in the (τ_e, τ_s) frame follows a straight line when changing the assistive force value F (Fig. 3).

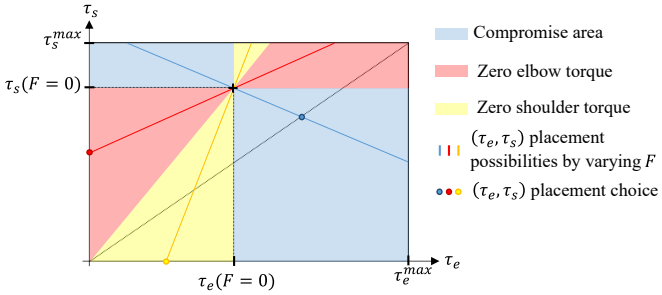

Fig. 3: Illustration of the Motor Ability Based (MAB) strategy for an arm pose where the point (τ_e, τ_s) without assistance $(F = 0)$ lies in the first quadrant.

This strategy computes F_g^* in two possible ways, depending on the upper-limb pose:

a) for some poses, there are no compromise to do: increasing F reduces both joint torques τ_e and τ_s (red and yellow regions in Fig. 3). The gravity compensation force F_g^* is here computed to zero one or the other torque while staying in the same quadrant;

b) other poses require a compromise between τ_e and τ_s: increasing F reduces one torque but increases the other one (blue region in Fig. 3). The gravity compensation force F_g^* is here computed to match the user's motor abilities in term of maximum joint torques, assumed to be τ_e^{max} and τ_s^{max}. In other words, F_g^* is computed to ensure that $\tau_e/\tau_s = \tau_e^{max}/\tau_s^{max}$.

3) Minimal Torque Norm (MTN) strategy: For this strategy, a quantity representing the global effort to maintain the upper-limb pose is required. As a first approach, we may want to minimize $\tau_e^2 + \tau_s^2$. However, each user has different motor abilities, so a coefficient α is introduced to put more or less load on the minimization of the shoulder torque compared to the elbow one. Thus, the gravity compensation force F_g^* is computed to minimize the "torque norm" T

$$F_g^* = \arg\min_F T = \arg\min_F (\tau_e^2 + \alpha\tau_s^2), \qquad (11)$$

with τ_e and τ_s expressed according to Eq. (3).

4) Monte Carlo Based (MCB) strategy: All of the previous strategies rely on a model of the upper-limb that we suppose to know perfectly. In practice, the BSIPs and current pose of the upper-limb as well as the assistive force applied to the forearm are not perfectly known. To take these uncertainties into account, a strategy based on a Monte Carlo simulation was created. The parameters required to compute the torques were supposed to be independent random variables uniformly distributed in an interval centered on their nominal value. The size of the intervals is equal to the parameters uncertainty. For a given upper-limb pose, 10000 set of parameters were randomly picked. Then, for each parameter set, the torque norm T is computed with different assistive force values with Eq. (11). For each value of F, the Probability Mass Function (PMF) of T is computed and F_g^* is chosen to minimize the PMF expectation.

III. EXPERIMENT AND RESULTS

The effectiveness of the four gravity compensation strategies to release the upper-limb was evaluated through an experiment with nine participants without NMDs (Fig. 4). See Table I for main characteristics of the participants. To evaluate the effectiveness of the strategies, the activity of six muscles involved in upper-limb movements (Biceps Brachii, Triceps Brachii, Deltoideus Anterior, Deltoideus Medius, Deltoideus Posterior and Trapezius Descendens) was monitored and post-processed to compute the mean effort index (MEI), inspired from [17] (see subsection III-C for more details). The gravity compensation force F_g^* was provided by a DAS prototype presented in subsection III-A while the participants performed static poses. An additional trial was performed without the DAS as control. More details

N	Gender, M/F	Age (y)	Height (m)	Weight (kg)
9	5/4	31 (22-45)	1.73 (1.65-1.85)	64 (53-74)

TABLE I: Participants main characteristics. Numerical data are presented as mean (min-max). M: male, F: female.

on the experimental protocol are given in subsection III-B. The statistical method and the results are presented in subsections III-D and III-E respectively. This study was approved by the Operational Committee for the Evaluation of Legal and Ethical Risks (OCELER) of the Inria institute.

A. Experimental setup

Participants are first equipped with six wireless EMG sensors (Delsys, Trigno) placed according to the SENIAM project recommendations. They are seated on a chair equipped with the DAS prototype (Fig. 4). This chair is adjusted in front of the panel with six target points used for repetitiveness of the static pose tasks between participants.

The DAS prototype follows the same architecture as the Edero DAS from Armon (Fig. 5). A BLDC motor (MyActuator, RMD X6-S2) and a force sensor made of strain gauges (Micro-Measurements, MMF307441) were used to implement a closed-loop force control. The strain gauges are glued on the aluminum alloy tube that links the armrest and the motor. The motor is attached to a mechanism with three articulated limbs thanks to 3D printed parts. The force sensor was calibrated by fitting a bending beam model for the aluminum alloy tube. An average filter with 40 samples was added to improve the quality of the force measurement signal. The closed-loop control and the data acquisition are ensured by a control board (dSpace, DS1104) with a 400 Hz sampling rate. A PI controller with a dead-zone at its input as well as an anti-windup is used to ensure that the desired gravity compensation force F_g^* is applied within a $\pm 2\,\mathrm{N}$ error range. After identifying the BLDC motor, the gain were tuned to guarantee stability and a $1s$ time response for step inputs. User upper-limb pose was estimated by measuring the configuration of the 3-limbs mechanism with potentiometers (parameter x_m in Fig. 2) and with the motor angle measurement α_m. It was assumed that $\alpha = 1$ for the MTN and MCB strategies (Eq. (11)), and $\tau_{e_+}^{max}/\tau_{s_+}^{max} = 0.7$ for the MAB strategy (according to maximum torque values used in the design of exoskeletons [18]).

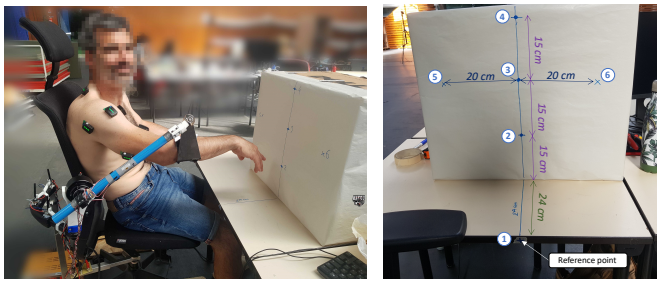

(a) A participant with the DAS. (b) The six target points.

Fig. 4: Experimental setup.

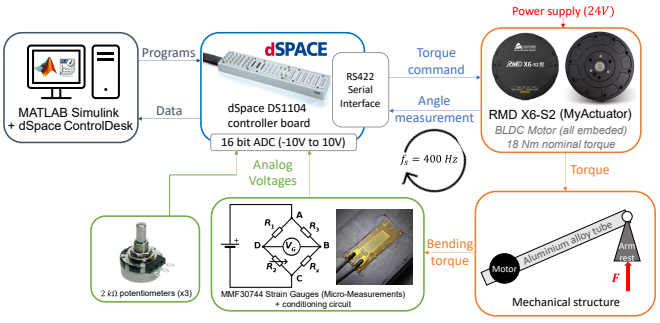

Fig. 5: DAS prototype hardware architecture

B. Experimental protocol

First, the participants received an information sheet with detailed information about the experiment and a description of the protocol. They were asked to sign a consent form to approve their agreement in the participation. Then, the required anthropometric data for the gravity compensation strategies (listed at the end of subsection II-B) are measured on the participants. They are then equipped with the EMG sensors (skin was shaved if required and washed with medical alcohol) and installed on the chair in front of the panel with the six target points, as in Fig. 4. The participants were firstly asked to perform the six static poses without the DAS to record the reference muscle activity signals. Next, they performed these static poses four times again to evaluate the four gravity compensation strategies. The strategy and the pose orders were randomized. The participants kept the static poses during seven seconds.

C. EMG signal processing and MEI computation

For each static pose, the average muscle activities were computed as the root mean square (RMS) value of the raw EMG signals in a five seconds window. For each measurement, it was checked that the assistive force F stays in the $\pm 2N$ range around the desired F_g^* force to discard outliers. For each pose p and muscle m, the mean value of the RMS recorded without DAS across the six poses ($\overline{\text{RMS}}_{0,m}$) was used for normalization (as suggested in [19]):

$$\overline{\text{RMS}}_{0,m} = \frac{1}{6}\sum_{p=1}^{6} \text{RMS}_{0,p,m}. \tag{12}$$

The normalized RMS values ($\text{nRMS}_{p,m}$) are then computed from $\overline{\text{RMS}}_{0,m}$ as

$$\text{nRMS}_{p,m} = \frac{\text{RMS}_{p,m}}{\overline{\text{RMS}}_{0,m}}. \tag{13}$$

As a score to assess the global effort to maintain the upper-limb in pose p, the MEI inspired from [17] was computed as the mean value of the nRMS across the six muscles:

$$\text{MEI}_p = \frac{1}{6}\sum_{m=1}^{6} \text{nRMS}_{p,m} \tag{14}$$

Differently from [17], no weighting was applied to compute the MEI. Indeed, a too high F_g^* force will increase the activity of muscles less physiologically involved in weight support (such as the Triceps Brachii), which may be attenuated by the weighting process.

D. Statistical method

The analysis of the MEI data was performed with R software (version 4.2.2, R Core Team). Three factors are influencing the MEI (the dependent variable): the pose, the gravity compensation strategy and the participant. Since the pose and strategy are considered as fixed effect whereas the participant as a random effect, the data was fitted to a linear mixed model using the "lme4" package with the formula

$$\text{MEI} \sim \text{Pose} + \text{Strategy} + (1|\text{Participant}). \tag{15}$$

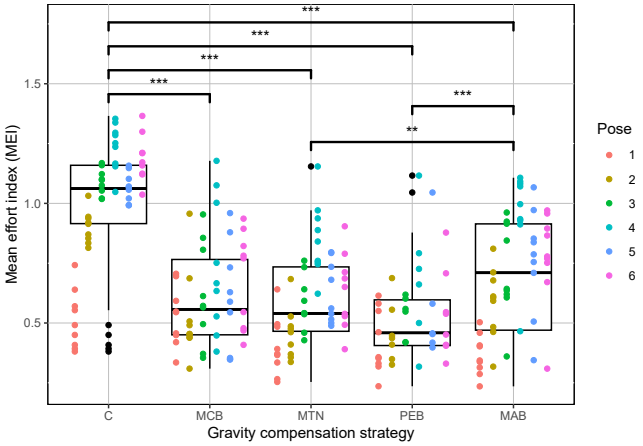

Fig. 6: MEI results across the four strategies and control trial without assistance (C). The results are grouped by strategy with boxplots. Significant differences are indicated.

To check the hypothesis of this model, a Shapiro–Wilk test was run on residuals which reveals they could be assumed to be normally distributed ($p > 0.2$). A Wald Chi-Squared test was then run to check global significance of the pose and the strategy on the MEI. Post-hoc analysis was then performed with Tukey tests to check significant differences between the poses and the strategies. p-values were adjusted with a single-step method. The statistical significance level was set to $p < 0.05$. Higher significance levels are indicated by '**' and '***' for $p < 0.01$ and $p < 0.001$ respectively.

E. Results

According to the Wald Chi-Squared test results, both pose and strategy have a significant influence on the MEI ($p < 0.001$). According to Tukey's test, all strategies reduce significantly the MEI ($p < 0.001$) compared to the control trial without assistance (C) as shown in Fig. 6. However, they do not have the same effectiveness. Indeed, MAB has a mean MEI of $+0.1$ (95% confidence interval of ± 0.08, $p < 0.01$) compared to MTN, and $+0.16$ (95% confidence interval of $\pm 0.09, p < 0.001$) compared to PEB. MCB has a lower median value than MAB (-0.15) but a greater interquartile compared to MTN ($+0.05$) and PEB ($+0.12$) strategies. No significant difference is observed between MCB, MTN and PEB, but PEB presents the lowest median value (0.46) and smallest interquartile range (0.19). Comparing the influence of the poses on the MEI, all of them are pairwise significantly different ($p < 0.01$) except from poses 3, 5 and 6 which are the three poses at the same height on the panel (Fig. 4). The median value of the MEI grouped by pose increases with the height of the target point, from 0.42 with pose 1 until 0.94 with pose 4. Lastly, looking at pose-wise impact of the strategies, pose 1 seems not affected by the different strategies while all the other poses present lower median values but also higher interquartile ranges with all strategies compared to the control trial with no assistance.

IV. DISCUSSION

The results show that the four gravity compensation strategies are efficient to release the upper-limb of people with no NMDs. The MAB strategy has the worst results in terms of mean MEI and inter-subject variability (Fig. 6). At the opposite, the PEB strategy shows the lowest mean MEI and inter-subject variability. The presence of outliers on poses 4 and 5 in the PEB strategy might come from participants which upper-limb was almost outstretched (i.e., near a singularity in the upper-limb model) which causes the desired F_g^* force to diverge since it is computed from the inverse Jacobian of the upper-limb, according to Eq. (8). This undesired behavior at the border of the upper-limb workspace will be corrected in future works. The four strategies are effective both for outstretched arm tasks (pose 3 to 6) requiring substantial effort, and for task with low muscle demand (pose 1) where the system does not overcompensate the arm weight. Moreover, the 2D model is efficient to support the arm in 3D since poses 3, 5 and 6 show no significant differences between them. However, all of the four strategies tend to increase the inter-subject variability. Since the strategies are based on a simplified model of the upper-limb, it may be hazardous to completely rely on it to generate the assistive force. The level of assistance might be adapted to every user, either by a global factor on the F_g^* force or by tuning the α coefficient for MTN and MCB strategies for instance. This may lead to better results for each participant and thus a lower inter-subject variability.

V. CONCLUSION

This paper presented a preliminary study which aimed to design a new framework to control active dynamic arm supports. We proposed four different gravity compensation strategies to support the upper-limb of people with neuromuscular disorders. These strategies are based on an upper-limb model and aim to reduce both elbow and shoulder torques with a single vertical force applied on the forearm by the arm support. The strategies were evaluated through an experiment with nine participants equipped with an active dynamic arm support prototype, in which the activity of six muscles was measured while performing static poses. The results show that the four strategies are efficient to support the upper-limb. The potential-energy-based (PEB) strategy shows the best results in terms of general arm release and inter-subject variability. In future works, the proposed gravity compensation strategies will be improved to be more suited to every users. The user intent will also be taken into account to implement the proposed force-based framework with gravity compensation. This framework will be then compared to position-based strategies and tested with people with neuromuscular disorders.

ACKNOWLEDGMENT

Authors would like to thank Eric Bazin for his support to develop the prototype, as well as Eric Courteille and Charles Pontonnier for their valuable advice to design and carry out the experimental protocol.

REFERENCES

[1] I. Naotunna, C. J. Perera, C. Sandaruwan, R. Gopura, and T. D. Lalitharatne, "Meal assistance robots: A review on current status, challenges and future directions," in *2015 IEEE/SICE International Symposium on System Integration (SII)*, 2015, pp. 211–216.

[2] C.-S. Chung, H. Wang, and R. A. Cooper, "Functional assessment and performance evaluation for assistive robotic manipulators: Literature review," *The Journal of Spinal Cord Medicine*, vol. 36, no. 4, pp. 273–289, 2013.

[3] M. Jansen, I. J. de Groot, N. van Alfen, and A. C. Geurts, "Physical training in boys with Duchenne Muscular Dystrophy: the protocol of the No Use is Disuse study," *BMC Pediatr*, vol. 10, p. 55, 2010.

[4] L. A. Van der Heide, B. van Ninhuijs, A. Bergsma, G. J. Gelderblom, D. J. van der Pijl, and L. P. de Witte, "An overview and categorization of dynamic arm supports for people with decreased arm function," *Prosthetics & Orthotics International*, vol. 38, no. 4, pp. 287–302, 2014.

[5] V. Longatelli, A. Antonietti, E. Biffi, E. Diella, M. G. D'Angelo, M. Rossini, F. Molteni, M. Bocciolone, A. Pedrocchi, and M. Gandolla, "User-centred assistive SystEm for arm Functions in neUromuscuLar subjects (USEFUL): a randomized controlled study," *J NeuroEngineering Rehabil*, vol. 18, no. 1, p. 4, 2021.

[6] M. A. Gull, S. Bai, and T. Bak, "A review on design of upper limb exoskeletons," *Robotics*, vol. 9, no. 1, p. 16, 2020, publisher: MDPI.

[7] J. M. N. Essers, A. Murgia, A. A. Peters, M. M. H. P. Janssen, and K. Meijer, "Recommendations for studies on dynamic arm support devices in people with neuromuscular disorders: a scoping review with expert-based discussion," *Disabil Rehabil Assist Technol*, pp. 1–14, 2020.

[8] J. Gantenbein, J. Dittli, J. T. Meyer, R. Gassert, and O. Lambercy, "Intention detection strategies for robotic upper-limb orthoses: a scoping review considering usability, daily life application, and user evaluation," *Frontiers in neurorobotics*, vol. 16, 2022, publisher: Frontiers Media SA.

[9] J. Lobo-Prat, P. N. Kooren, M. M. H. P. Janssen, A. Q. L. Keemink, P. H. Veltink, A. H. A. Stienen, and B. F. J. M. Koopman, "Implementation of EMG- and Force-Based Control Interfaces in Active Elbow Supports for Men With Duchenne Muscular Dystrophy: A Feasibility Study," *IEEE Trans. Neural Syst. Rehabil. Eng.*, vol. 24, no. 11, pp. 1179–1190, 2016.

[10] V. Zatsiorsky, "The mass and inertia characteristics of the main segments of the human body," *Biomechanics*, pp. 1152–1159, 1983.

[11] P. de Leva, "Adjustments to Zatsiorsky-Seluyanov's segment inertia parameters," *Journal of Biomechanics*, vol. 29, no. 9, pp. 1223–1230, 1996.

[12] J. L. Durkin and J. J. Dowling, "Analysis of Body Segment Parameter Differences Between Four Human Populations and the Estimation Errors of Four Popular Mathematical Models," *Journal of Biomechanical Engineering*, vol. 125, no. 4, pp. 515–522, 2003.

[13] D. A. Winter, *Biomechanics and motor control of human movement*, 4th ed. Hoboken, N.J: Wiley, 2009.

[14] Z. Merrill, S. Perera, and R. Cham, "Predictive regression modeling of body segment parameters using individual-based anthropometric measurements," *Journal of Biomechanics*, vol. 96, p. 109349, 2019.

[15] R. L. Whittaker, M. E. Vidt, R. M. Lockley, M. Mourtzakis, and C. R. Dickerson, "Upper extremity and trunk body segment parameters are affected by BMI and sex," *Journal of Biomechanics*, vol. 117, p. 110230, 2021.

[16] E. Palazzi, L. Luzi, E. Dimo, M. Meneghetti, R. Vicario, R. F. Luzia, R. Vertechy, and A. Calanca, "An Affordable Upper-Limb Exoskeleton Concept for Rehabilitation Applications," *Technologies*, vol. 10, no. 1, p. 22, 2022.

[17] F. Just, Özen, S. Tortora, V. Klamroth-Marganska, R. Riener, and G. Rauter, "Human arm weight compensation in rehabilitation robotics: efficacy of three distinct methods," *Journal of NeuroEngineering and Rehabilitation*, vol. 17, no. 1, p. 13, 2020.

[18] N. Tsagarakis, D. Caldwell, and G. Medrano-Cerda, "A 7 DOF pneumatic muscle actuator (pMA) powered exoskeleton," in *8th IEEE International Workshop on Robot and Human Interaction. RO-MAN '99 (Cat. No.99TH8483)*. Pisa, Italy: IEEE, 1999, pp. 327–333.

[19] P. Konrad, "The abc of emg," *A practical introduction to kinesiological electromyography*, vol. 1, no. 2005, pp. 30–5, 2005.